

Metal–Organic Frameworks

International Edition: DOI: 10.1002/anie.201607271

German Edition: DOI: 10.1002/ange.201607271

Copper–Organic Framework Fabricated with CuS Nanoparticles: Synthesis, Electrical Conductivity, and Electrocatalytic Activities for Oxygen Reduction Reaction

Keumnam Cho, Sung-Hwan Han, and Myunghyun Paik Suh*

Abstract: To apply electrically nonconductive metal–organic frameworks (MOFs) in an electrocatalytic oxygen reduction reaction (ORR), we have developed a new method for fabricating various amounts of CuS nanoparticles (nano-CuS) in/on a 3D Cu–MOF, $[\text{Cu}_3(\text{BTC})_2(\text{H}_2\text{O})_3]$ (BTC = 1,3,5-benzenetricarboxylate). As the amount of nano-CuS increases in the composite, the electrical conductivity increases exponentially by up to circa 10^9 -fold, while porosity decreases, compared with that of the pristine Cu–MOF. The composites, nano-CuS(*x* wt %>@Cu-BTC, exhibit significantly higher electrocatalytic ORR activities than Cu-BTC or nano-CuS in an alkaline solution. The onset potential, electron transfer number, and kinetic current density increase when the electrical conductivity of the material increases but decrease when the material has a poor porosity, which shows that the two factors should be finely tuned by the amount of nano-CuS for ORR application. Of these materials, CuS(28 wt %>@Cu-BTC exhibits the best activity, showing the onset potential of 0.91 V vs. RHE, quasi-four-electron transfer pathway, and a kinetic current density of 11.3 mA cm^{-2} at 0.55 V vs. RHE.

Development of electrocatalysts for the oxygen reduction reaction (ORR) in fuel cells or metal–air batteries is a currently important research area.^[1,2] So far, platinum-based catalysts have shown the best activity for the ORR,^[3,4] but they are expensive and not abundant, and thus they should be replaced with other inexpensive electrocatalysts. Metal–organic frameworks (MOFs) have versatile structures and high porosity^[5] and can be applied in gas storage,^[6–8] gas separation,^[9,10] and catalysis.^[11] MOFs have been also utilized as the matrixes for the fabrication of metal or metal oxide nanoparticles (NPs).^[7,12–21] Additionally, MOFs could be applied as electrocatalysts for the ORR, since they contain abundant pores that can facilitate oxygen and water transfer and many metal sites that can be involved in the catalytic reactions as the active sites. However, most MOFs are electrical insulators and their application as electrocatalysts is limited. Recently, a few conducting MOFs have been

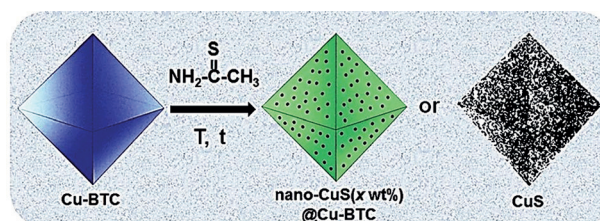
synthesized and applied in the electrochemical ORR.^[22,23] Although some efforts have been made to utilize non-conducting MOFs or their composites of graphene oxide, reduced graphene oxide, and MnO_2 as electrochemical ORR catalysts,^[24–33] their performances were not so excellent. To develop efficient MOF-based ORR electrocatalysts, we have tried to increase the electrical conductivity of MOFs, in particular, by fabricating nanosized metal-compound particles in their pores. We have chosen copper sulfide as the pore inclusion compound because it has low surface resistivity (10^{-4} – $1 \text{ } \Omega \text{ cm}$).^[34] Although various metal and metal oxide nanoparticles have been prepared in the MOFs,^[7,12–21] the reports of metal sulfide nanoparticles fabricated in MOFs are still rare.

Herein, we report for the first time, to the best of our knowledge, a method for fabricating various amounts of nano-CuS in/on a 3D MOF, which gives rise to nano-CuS(*x* wt %>@Cu-BTC (*x* = 1.4, 5.3, 8.8, 28, and 56) and nano-CuS(99 wt %) (Scheme 1). The series of composites were prepared by a simple solution infiltration method, using Cu-BTC as a sacrificial template and a EtOH solution of thioacetamide as the sulfide source^[35] with the control of the reaction time and temperature. There have been some reports of the synthesis of metal oxides using MOFs as sacrificial templates,^[36–38] but none of metal sulfide. In most of those cases, template MOFs were completely consumed during the formation of the NPs, and only NPs and/or carbon was left. The present solution infiltration method enables the amount of CuS formed in/on the MOF to be easily controllable. By increasing the amount of nano-CuS in the material, electrical conductivity increases by up to 10^9 -fold, while porosity decreases, compared to those of the pristine Cu-BTC. In ORR, the catalytic performance of the composite materials significantly increases, as shown by increases in the onset voltage, electron transfer number, and kinetic current density, compared with those of the pristine MOF and nano-CuS. This is due to the synergistic effect of two different materials, which provide the porosity and the electrical

[*] K. Cho, Prof. S.-H. Han, Prof. M. P. Suh
Department of Chemistry, Hanyang University
Seoul 04763 (Republic of Korea)
E-mail: mpsuh@snu.ac.kr

Prof. M. P. Suh
Department of Chemistry, Seoul National University
Seoul 08826 (Republic of Korea)

Supporting information and the ORCID identification number(s) for the author(s) of this article can be found under:
<http://dx.doi.org/10.1002/anie.201607271>.



Scheme 1. Synthesis of nano-CuS(*x* wt %>@Cu-BTC and nano-CuS(99 wt %).

conductivity, respectively. In the present composite materials, nano-CuS(28 wt %)@Cu-BTC shows the best ORR activity.

A fixed amount of as-synthesized $[\text{Cu}_3(\text{BTC})_2 \cdot (\text{H}_2\text{O})_3]^{[39]}$ (Cu-BTC) was immersed in an anhydrous EtOH solution of thioacetamide with a fixed concentration for 1 and 12 h at 10 °C, and for 1, 3, 5, and 12 h at 30 °C (for the detailed procedure, see the Supporting Information). The reaction afforded the composites of nano-CuS(*x* wt %)@Cu-BTC (*x* = 1.4, 5.3, 8.8, 28, and 56) and nano-CuS(99 wt %) containing a small amount of insoluble H₃BTC (Supporting Information, Tables S1 and S2). The field emission-scanning electron microscopy (FE-SEM) and transmission electron microscopy (TEM) images show that nano-CuS forms in and on the MOF, maintaining the octahedral crystal shape of Cu-BTC (Figure 1 and the Supporting Information, Table S1). The reason why the crystal shape is conserved in the present composites is not

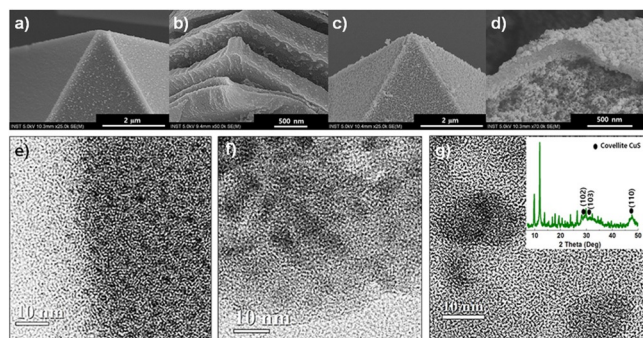


Figure 1. FE-SEM images of a) nano-CuS(5.3 wt %)@Cu-BTC, b) after crystal (a) was cut by the X-ray beam, c) nano-CuS(28 wt %)@Cu-BTC, and d) after crystal (c) was cut by the X-ray beam. e–g) TEM images of (e) nano-CuS(5.3 wt %)@Cu-BTC, f) nano-CuS(28 wt %)@Cu-BTC, and g) nano-CuS(56 wt %)@Cu-BTC. Inset: PXRD pattern of (g).

clear, but there have been some reports of the conservation of the morphologies of MOF crystals during the thermal transformation to CuO/Cu₂O@C and the formation of mesoporous Co-Ni-O.^[40,41] The amounts of nano-CuS in the composites were estimated based on the elemental analysis (EA) data, which were obtained after drying the samples at 90 °C for 24 h. In particular, for the EA data of sulfur, we assumed that nano-CuS had a covellite phase with a Cu²⁺ oxidation state as evidenced by powder X-ray diffraction (PXRD), HRTEM, selected-area electron diffraction (SAED), and X-ray photoelectron spectroscopy (XPS) data (Supporting Information, Figure S1 and Table S2).

The amounts (1.4–99 wt %) and average sizes (1.0–43 nm) of nano-CuS in the composites depend on the reaction time and temperature (Supporting Information, Table S1 and Figures S2 and S3). Furthermore, the formation of CuS is affected by the hydration state of the MOF. When we performed the reaction at 30 °C for 3 h in the dried EtOH solution of dried thioacetamide with the activated Cu-BTC, which still has coordinated water molecules but no guest water, a composite containing only 1.1 wt % of nano-CuS was formed (see the Supporting Information), in contrast with the formation of 28 wt % CuS from the as-synthesized MOF. In general, the amount and size of nano-CuS increase with

increasing reaction time at a fixed temperature. However, the size of nano-CuS formed at 30 °C is much smaller than that formed at 10 °C. Furthermore, when the reaction was performed at 60 °C or 80 °C for 2 h, PXRD patterns of the products showed only the peaks corresponding to CuS, indicating that almost all Cu-BTC was converted to CuS (Supporting Information, Figure S4). This is contrary to our previous reports, in which NPs of Ag, Au, and Pd were produced in redox active coordination polymers (PCPs) or MOFs by immersing them in Ag⁺, Au³⁺, and Pd²⁺ solutions. In those cases, the amount of NPs was affected by the reaction time, but their size was independent of the reaction conditions.^[12,14–17]

To produce nano-CuS in/on the Cu-BTC, thioacetamide (estimated size, 4.1 × 3.6 Å) should diffuse to the pores of the MOF (with pore diameters of 3.5, 5.0, and 9.0 Å^[42]), and then react with water molecules contained in the MOF to form H₂S gas [Eq. (1)]. Then, H₂S gas would react with Cu²⁺ ions of the Cu-BTC to afford the composite materials [Eq. (2)].



To verify the suggested mechanism, we performed experiments by using H₂S gas. When the EtOH (anhydrous) suspension of as-synthesized Cu-BTC was bubbled with H₂S gas at 30 °C for 3 h, CuS(37 wt %)@Cu-BTC resulted. Moreover, when MOF powder was exposed to H₂S gas at 30 °C for 3 h, CuS(24 wt %)@Cu-BTC was formed (see the Supporting Information). Although the hydrolysis rate of thioacetamide in neutral water is very slow,^[43] we believe that it becomes much faster in the pores of the MOF as suggested in the Supporting Information, Figure S5. The Cu, O, and S elemental mapping data obtained by scanning TEM (Supporting Information, Figure S6) indicate that as the reaction time increases, the oxygen content of the product decreases while the sulfur content increases. This clearly shows that the Cu-MOF acts as a sacrificial matrix, which loses more BTC ligand and forms more nano-CuS as the reaction proceeds.

The PXRD patterns (Supporting Information, Figure S7) indicate that the MOF framework structure is retained even after the formation of nano-CuS, whose size is much bigger than the pore sizes of the MOF. To explain this, we calculated the ratio of the volumes of nano-CuS and the framework skeleton in nano-CuS(28 wt %)@Cu-BTC. Assuming that all the nano-CuS destroy the framework skeleton, they would destroy a maximum 22% of the framework by volume, implying that a significant part of the Cu-BTC framework remains in the composites (for detailed calculations, see Supporting Information). Similar retention of the network structures was also observed previously in the cases of Ag, Au, Pd, and Mg NPs formation in PCPs and MOFs.^[7,12,14–17] Fourier transform infrared (FTIR) spectra also supported the presence of Cu-BTC in the composites (Supporting Information, Figure S8 and Table S3).

When the MOF was removed from CuS(8.8 wt %)@Cu-BTC, which was prepared at 10 °C with a reaction time of 12 h, by using 0.1M HCl, big CuS nanorods (size, 104 ×

345 nm) were isolated (Supporting Information, Figure S1). This is contrary to the other products formed at 30 °C, in which the sizes of nano-CuS are much smaller. TEM images reveal that big nanorods are formed by the aggregation of much smaller NPs (17 nm) and nanorods (11 × 25 nm). The lattice fringe spacing in HRTEM and SAED images indicate that the nano-CuS has a covellite phase (Supporting Information, Figure S1).^[44] The PXRD patterns of the isolated nano-CuS as well as that of nano-CuS(99 wt%) show the peaks at $2\theta = 29.2^\circ$ (102), 31.8° (103), and 47.9° (110), being coincident with those of covellite CuS (JCPDS 06-0464). The XPS data show two peaks at 951.8 and 931.9 eV for Cu 2p, with the separation of 19.9 eV, indicating a +2 oxidation state for the Cu ion.^[45] The peak for S 2p is seen at 162.3 eV, also being coincident with the reported value.^[45]

To see the generality of the present approach, similar reactions were conducted with other MOFs, [Cu₂(OH)(bipy)₂(BTC)₃·2H₂O (bipy = 2,2'-bipyridine)^[46] and [Co₃BTC₂]₁₂H₂O^[47]. Preliminary results indicate the formation of metal sulfide nanoparticles in/on the corresponding MOFs (Supporting Information, Figures S9–S11).

The N₂ gas adsorption and desorption isotherms were measured at 77 K. BET surface areas of nano-CuS-(*x* wt%)-Cu-BTC decrease as the amount of nano-CuS increases, 1740, 1710, 1660, 1570, 1140, and 110 m² g⁻¹, respectively, for the MOF materials containing 0, 1.4, 5.3, 8.8, 28, and 56 wt% nano-CuS (Table 1, Figure 2, and the Supporting Information, Figure S12). The pore distribution curves obtained by BELMaster software (MicrotracBEL, Japan) based on the nonlocalized density functional theory and grand canonical Monte Carlo method (NLDFT/GCMC) indicate that the pore sizes of the composites are much bigger than those (0.63 and 0.91 nm) of the pristine Cu-BTC (Supporting Information, Figure S12 and Table S4). In particular, heavily CuS loaded samples, nano-CuS(56 wt%)-Cu-BTC and nano-CuS(99 wt%), even contain macropores (size > 50 nm), which might be attributed to their very small BET surface areas, compared with the other composites, together with pore space occupation by the greater amount of nano-CuS.

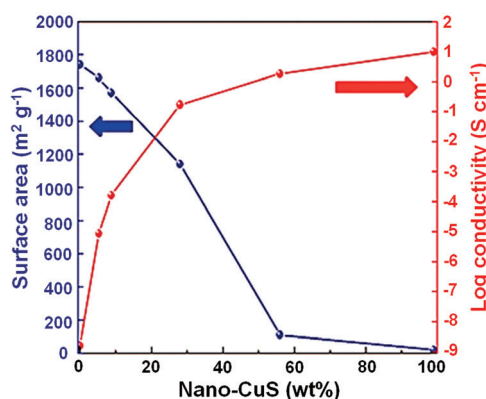


Figure 2. BET surface area and electrical conductivity (log scale) versus amount of nano-CuS contained in the Cu-MOF.

Electrical conductivity was measured by the four-probe method at 25 °C, using pellet samples. At least 50 data points were collected at different positions for each sample by using 2–3 pellets, and the average values are summarized in Table 1. The composites exhibit highly (up to 10⁹-fold) enhanced electrical conductivity (4.7×10^{-8} – 1.8 Scm^{-1}) compared with that ($1.6 \times 10^{-9} \text{ Scm}^{-1}$) of Cu-BTC as shown in Figure 2. The electrical conductivity increases as the amount of nano-CuS increases. In particular, those for the materials containing 28 and 56 wt% nano-CuS are 0.17 Scm^{-1} and 1.8 Scm^{-1} , respectively, which are circa 10⁸- and 10⁹-fold higher than that of the pristine MOF. The electrical conductivity of nano-CuS(99 wt%) is 9.6 Scm^{-1} . These are comparable to the values of semiconductors and the previously reported conducting MOF, Ni₃(HITP)₂.^[48]

To evaluate the electrocatalytic activities for the ORR, we performed linear sweep voltammetry (LSV) as well as cyclic voltammetry (CV) in O₂-saturated 0.1 M KOH (pH 13.4) by using a GC disk electrode loaded with composite catalyst and carbon black (CB) (for details, see Supporting Information). The LSV curves are shown in Figure 3 and the Supporting Information, Figure S15, and the data are summarized in Table 1. The onset potential (E_{onset}) for the ORR was greatly

Table 1: BET surface area, electrical conductivity, and electrocatalytic activities of various materials.

| Material | BET [m ² /g] | Conductivity ^[a] [S cm ⁻¹] | E_{onset} ^[e] [V vs. RHE] | e-transfer number [<i>n</i>] | Reference |
|--|-------------------------|---|---|--------------------------------|-----------|
| Carbon black (CB) Cu-BTC | – | – | 0.71 ^[e] | 1.74 ^[c,f] | This work |
| | 1740 | 1.6×10^{-9} ^[b,c] | 0.76 ^[e] | 2.05 ^[c,f] | This work |
| Nano-CuS(1.4 wt%)-Cu-BTC | 1710 | 4.7×10^{-8} ^[b,c] | 0.79 ^[e] | 2.38 ^[c,f] | This work |
| Nano-CuS(5.3 wt%)-Cu-BTC | 1660 | 8.8×10^{-6} ^[b,c] | 0.80 ^[e] | 2.67 ^[c,f] | This work |
| Nano-CuS(8.8 wt%)-Cu-BTC | 1570 | 1.6×10^{-4} ^[b,c] | 0.85 ^[e] | 3.30 ^[c,f] | This work |
| Nano-CuS(28 wt%)-Cu-BTC | 1140 | 1.7×10^{-1} ^[b,c] | 0.91 ^[e] | 3.82 ^[c,f] | This work |
| Nano-CuS(56 wt%)-Cu-BTC | 110 | 1.8 ^[b,c] | 0.86 ^[e] | 2.64 ^[c,f] | This work |
| Nano-CuS(99 wt%) | 20 | 9.6 ^[b,c] | 0.78 ^[e] | 3.30 ^[c,f] | This work |
| Pt(20 wt%)/C | – | – | 1.00 ^[e] | 4.02 ^[c,f] | This work |
| Ni ₃ (HITP) ₂ ^[g] | – | 2, ^[b] 40 ^[d] | 0.82 ^[c,e] | 2.25 | [23, 48] |
| TCNQ@Cu ₃ (BTC) ₂ ^[h] | – | 0.07 | – | – | [49] |
| Cu-bipy-btc ^[i] | – | – | 0.50 ^[j] | 3.8 ^[k] | [24] |
| Graphene–Porphyrin Fe-MOF composite | – | – | 0.93 ^[e] | 3.82 ^[l] | [26] |

[a] Average value of 50 data points measured at 25 °C (Supporting Information, Table S5). [b] Pellet samples. [c] Measured at room temperature. [d] Film samples. [e] Measured in 0.1 M KOH. [f] Obtained at 0.55 V vs. RHE. [g] 2,3,6,7,10,11-hexamino-triphenylene. [h] 7,7,8,8-tetracyanoquinodimethane. [i] Copper(II)-2,2'-bipyridinebenzene-1,3,5-tricarboxylate. [j] Measured in 0.10 M phosphate buffer (pH 6.0). [k] Obtained from the ratio of ring-disk current. [l] Obtained at –0.65 V vs. Ag/AgCl.

affected by the amount of nano-CuS contained in the catalysts. As the amount of nano-CuS increases and thus the electrical conductivity increases, E_{onset} shifts to more positive potentials, 0.79, 0.80, 0.85, and 0.91 V vs. RHE, respectively, for the samples containing 1.4, 5.3, 8.8, and 28 wt % nano-CuS. These onset potentials are higher than that of pristine Cu-BTC or nano-CuS(99 wt %). However, as seen in the case of CuS(56 wt %>@Cu-BTC, when too much nano-CuS is loaded into the MOF, porosity becomes very poor ($110 \text{ m}^2 \text{ g}^{-1}$) and the onset potential starts to decrease (0.86 V). This suggests that both the electrical conductivity and porosity of the composite catalysts play important roles in the electrocatalytic ORR. However, because the two factors behave oppositely with respect to the amount of CuS loaded in/on the MOF (Figure 2), they should be finely tuned by the amount of nano-CuS fabricated in/on the MOF. It should be noted that in the LSV curves, the current densities of the composite catalysts become saturated near 0.4–0.5 V and then

increase again at $V < 0.4$ V owing to H_2 evolution or catalyst decomposition, while those of CB and commercial Pt/C remain saturated. In the CV data as well (Supporting Information, Figure S16), as the amount of nano-CuS in the composite increases, the ORR peak shifts toward a more positive potential.

Koutecky–Levich (K–L) plots were prepared (Supporting Information, Figures S17 and S18) from the LSV data measured at various electrode rotating speeds, and the electron transfer numbers and kinetic current density were estimated from the plots^[50] (see Supporting Information). The K–L plots show good linearity at 0.40–0.55 V vs. RHE, suggesting first-order reaction kinetics for the ORR. The electron transfer numbers in ORR catalyzed by Cu-BTC and the composites are nearly constant in the range of 0.40–0.55 V (Figure 3). The electron transfer numbers for CB and Cu-BTC are 1.74 and 2.05, respectively, at 0.55 V, implying that ORR proceeds through the two-electron transfer pathway with these catalysts. This is not good for the application since peroxide involves corrosion or premature degradation of the cells. The electron transfer numbers for the catalysts loaded with 1.4, 5.3, 8.8, 28, and 56 wt % nano-CuS are 2.38, 2.67, 3.30, 3.82, 2.61, respectively, at 0.55 V. In particular, CuS-(28 wt %>@Cu-BTC shows a quasi-four-electron transfer pathway ($n = 3.82$) in the ORR, and it would not involve these problems. This is in contrast to a recent report for the electrically conducting MOF, $\text{Ni}_3(\text{HITP})_2$, with which the ORR occurs only by a two-electron reduction ($n = 2.25$).^[23] Detailed mechanistic studies for the ORR with the present catalysts are underway. As for the kinetic current density (Figure 3), all nano-CuS(x wt %>@Cu-BTC afforded enhanced values compared with Cu-BTC and nano-CuS-(99 wt %). For example, the values for the kinetic current density at 0.55 V are 6.63, 6.76, 10.1, and 11.3 mA cm^{-2} for 1.4, 5.3, 8.8, and 28 wt % nano-CuS-loaded composites, respectively. These are much higher than those of Cu-BTC and nano-CuS(99 wt %), 3.46 and 3.36 mA cm^{-2} , respectively. However, a 56 wt % nano-CuS-loaded sample that has a much reduced surface area affords a significantly lower kinetic current density (5.35 mA cm^{-2} at 0.55 V) than the other composites. This again suggests that both the electrical conductivity and porosity of the composite catalysts should be high for the ORR application. Compared with commercial 20 wt % Pt/C (20.1 mA cm^{-2} at 0.55 V), the present materials display lower kinetic current densities. Current–time chronoamperometry data (Supporting Information, Figure S19) indicate that the composite catalysts retain more than 75 % of the initial current density after 10000 s, which suggests relatively high stability. However, to replace platinum-based catalysts in fuel cells with the present type of composites, systematic studies should be conducted to increase the kinetic current density as well as stability.

In conclusion, we have fabricated various amounts of CuS nanoparticles in/on a nonconductive 3D Cu-MOF and showed how the electrical conductivity, porosity, and electrocatalytic ORR activity of the materials are affected by the amount of nano-CuS. In particular, electrical conductivity of the composite materials could be increased by circa 10^3 -fold, to the values of semiconductors. The materials afford more positive

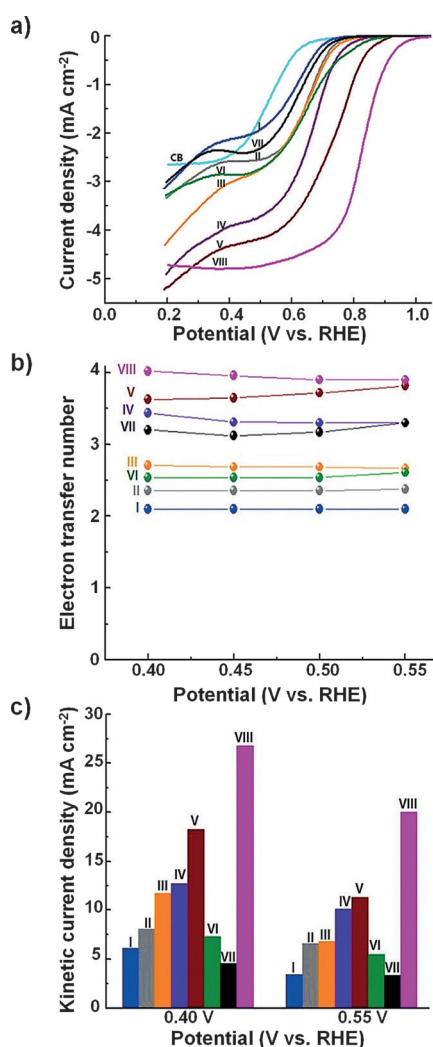


Figure 3. a) LSV measured in O_2 -saturated 0.1 M KOH at rt. Electrode rotating speed = 1600 rpm, scan rate = 10 mVs^{-1} . b) Electron transfer numbers at 0.40–0.55 V vs. RHE, c) kinetic current density at 0.40 V and 0.55 V vs. RHE for Cu-BTC (I), nano-CuS(1.4 wt %>@Cu-BTC (II), nano-CuS(5.3 wt %>@Cu-BTC (III), nano-CuS(8.8 wt %>@Cu-BTC (IV), nano-CuS(28 wt %>@Cu-BTC (V), nano-CuS(56 wt %>@Cu-BTC (VI), nano-CuS(99 wt %) (VII), and commercial 20 wt % Pt/C (VIII).

onset potentials, higher electron transfer numbers, and higher kinetic current densities in the electrocatalytic oxygen reduction than the pristine MOF, although they are still lower than commercial Pt/C. Considering the versatility of MOFs and metal sulfides having different physical properties, this work provides a new paradigm for the synthesis of many other composite materials, and the systematic optimization of the materials could lead to ORR electrocatalysts that can practically replace platinum-based catalysts in fuel cells.

Acknowledgements

This work was supported by National Research Foundation of Korea (NRF) Grant funded by the Korean Government (MEST) (No. 2005-0093842 and No. 2013R1A1A2009768). The authors express sincere thanks to Prof. Taek Dong Chung and Dr. Jinho Chang for helpful discussions.

Keywords: copper sulfide · electrocatalysis · metal-organic frameworks · nanoparticles · oxygen reduction

How to cite: *Angew. Chem. Int. Ed.* **2016**, *55*, 15301–15305
Angew. Chem. **2016**, *128*, 15527–15531

- [1] Y. Jiao, Y. Zheng, M. Jaroniec, S. Z. Qiao, *Chem. Soc. Rev.* **2015**, *44*, 2060–2086.
- [2] F. Cheng, J. Chen, *Chem. Soc. Rev.* **2012**, *41*, 2172–2192.
- [3] C. Cui, L. Gan, M. Heggen, S. Rudi, P. Strasser, *Nat. Mater.* **2013**, *12*, 765–771.
- [4] B. Lim, M. Jiang, P. H. Camargo, E. C. Cho, J. Tao, X. Lu, Y. Zhu, Y. Xia, *Science* **2009**, *324*, 1302–1305.
- [5] H. Furukawa, K. E. Cordova, M. O’Keeffe, O. M. Yaghi, *Science* **2013**, *341*, 1230444.
- [6] M. P. Suh, H. J. Park, T. K. Prasad, D.-W. Lim, *Chem. Rev.* **2012**, *112*, 782–835.
- [7] D. W. Lim, J. W. Yoon, K. Y. Ryu, M. P. Suh, *Angew. Chem. Int. Ed.* **2012**, *51*, 9814–9817; *Angew. Chem.* **2012**, *124*, 9952–9955.
- [8] D. W. Lim, S. A. Chyun, M. P. Suh, *Angew. Chem. Int. Ed.* **2014**, *53*, 7819–7822; *Angew. Chem.* **2014**, *126*, 7953–7956.
- [9] D. M. D’Alessandro, B. Smit, J. Long, *Angew. Chem. Int. Ed.* **2010**, *49*, 6058–6082; *Angew. Chem.* **2010**, *122*, 6194–6219.
- [10] J.-R. Li, J. Sculley, H.-C. Zhou, *Chem. Rev.* **2012**, *112*, 869–932.
- [11] A. H. Chughtai, N. Ahmad, H. A. Younus, A. Laypkov, F. Verpoort, *Chem. Soc. Rev.* **2015**, *44*, 6804–6849.
- [12] H. R. Moon, D.-W. Lim, M. P. Suh, *Chem. Soc. Rev.* **2013**, *42*, 1807–1824.
- [13] S. Hermes, M. K. Schröder, R. Schmid, L. Khodeir, M. Muhler, A. Tissler, R. W. Fischer, R. A. Fischer, *Angew. Chem. Int. Ed.* **2005**, *44*, 6237–6241; *Angew. Chem.* **2005**, *117*, 6394–6397.
- [14] H. R. Moon, J. H. Kim, M. P. Suh, *Angew. Chem. Int. Ed.* **2005**, *44*, 1261–1265; *Angew. Chem.* **2005**, *117*, 1287–1291.
- [15] M. P. Suh, H. R. Moon, E. Y. Lee, S. Y. Jang, *J. Am. Chem. Soc.* **2006**, *128*, 4710–4718.
- [16] Y. E. Cheon, M. P. Suh, *Chem. Eur. J.* **2008**, *14*, 3961–3967.
- [17] Y. E. Cheon, M. P. Suh, *Angew. Chem. Int. Ed.* **2009**, *48*, 2899–2903; *Angew. Chem.* **2009**, *121*, 2943–2947.
- [18] F. Schröder, D. Esken, M. Cokoja, M. W. van den Berg, O. I. Lebedev, G. Van Tendeloo, B. Walaszek, G. Buntkowsky, H.-H. Limbach, B. Chaudret, *J. Am. Chem. Soc.* **2008**, *130*, 6119–6130.
- [19] R. J. T. Houk, B. W. Jacobs, F. E. Gabaly, N. N. Chang, A. A. Talin, D. D. Graham, S. D. House, I. M. Robertson, M. D. Allendorf, *Nano Lett.* **2009**, *9*, 3413–3418.
- [20] G. Lu, S. Li, Z. Guo, O. K. Farha, B. G. Hauser, X. Qi, Y. Wang, X. Wang, S. Han, X. Liu, *Nat. Chem.* **2012**, *4*, 310–316.
- [21] P. Falcato, R. Ricco, A. Yazdi, I. Imaz, S. Furukawa, D. Maspoch, R. Ameloot, J. D. Evans, C. J. Doonan, *Coord. Chem. Rev.* **2016**, *307*, 237–254.
- [22] L. Sun, M. G. Campbell, M. Dincă, *Angew. Chem. Int. Ed.* **2016**, *55*, 3566–3579; *Angew. Chem.* **2016**, *128*, 3628–3642.
- [23] E. M. Miner, T. Fukushima, D. Sheberla, L. Sun, Y. Surendranath, M. Dincă, *Nat. Commun.* **2016**, *7*, 10942.
- [24] J. Mao, L. Yang, P. Yu, X. Wei, L. Mao, *Electrochem. Commun.* **2012**, *19*, 29–31.
- [25] M. Jahan, Z. Liu, K. P. Loh, *Adv. Funct. Mater.* **2013**, *23*, 5363–5372.
- [26] M. Jahan, Q. Bao, K. P. Loh, *J. Am. Chem. Soc.* **2012**, *134*, 6707–6713.
- [27] D. Wu, Z. Guo, X. Yin, Q. Png, B. Tu, L. Zhang, Y.-G. Wang, Q. Li, *Adv. Mater.* **2014**, *26*, 3258–3262.
- [28] H. Wang, F. Yin, B. Chen, G. Li, *J. Mater. Chem. A* **2015**, *3*, 16168–16176.
- [29] H. Wang, F. Yin, G. Li, B. Chen, Z. Wang, *Int. J. Hydrogen Energy* **2014**, *39*, 16179–16186.
- [30] X. He, F. Yin, G. Li, *Int. J. Hydrogen Energy* **2015**, *40*, 9713–9722.
- [31] M. Jiang, L. Li, D. Zhu, H. Zhang, X. Zhao, *J. Mater. Chem. A* **2014**, *2*, 5323–5329.
- [32] F. Yin, G. Li, H. Wang, *Catal. Commun.* **2014**, *54*, 17–21.
- [33] P. Miao, G. Li, G. Zhang, H. Lu, *J. Energy Chem.* **2014**, *23*, 507–512.
- [34] J. Johansson, J. Kostamo, M. Karppinen, L. Niinistö, *J. Mater. Chem.* **2002**, *12*, 1022–1026.
- [35] D. V. Shinde, S. A. Patil, K. Cho, D. Y. Ahn, N. K. Shrestha, R. S. Mane, J. K. Lee, S. H. Han, *Adv. Funct. Mater.* **2015**, *25*, 5739–5747.
- [36] J. Jiang, C. Zhang, L. Ai, *Electrochim. Acta* **2016**, *208*, 17–24.
- [37] Y. Wang, C. Wang, Y. Wang, H. Liu, Z. Huang, *J. Mater. Chem. A* **2016**, *4*, 5428–5435.
- [38] H. Niu, S. Liu, Y. Cai, F. Wu, X. Zhao, *Microporous Mesoporous Mater.* **2016**, *219*, 48–53.
- [39] J. Liu, Y. Wang, A. I. Benin, P. Jakubczak, R. R. Willis, M. D. LeVan, *Langmuir* **2010**, *26*, 14301–14307.
- [40] A.-Y. Kim, M. K. Kim, K. Cho, J.-Y. Woo, Y. Lee, S.-H. Han, D. Byun, W. Choi, J. K. Lee, *ACS Appl. Mater. Interfaces* **2016**, *8*, 19514–19523.
- [41] H. Li, M. Liang, W. Sun, Y. Wang, *Adv. Funct. Mater.* **2016**, *26*, 1098–1103.
- [42] A. Vishnyakov, P. I. Ravikovitch, A. V. Neimark, M. Bülow, Q. M. Wang, *Nano Lett.* **2003**, *3*, 713–718.
- [43] O. M. Pesters, C. J. De Ranter, *J. Chem. Soc. Perkin Trans. 2* **1976**, 1062–1065.
- [44] S. Thongtem, C. Wichasilp, T. Thongtem, *Mater. Lett.* **2009**, *63*, 2409–2412.
- [45] I. Nakai, Y. Sugitani, K. Nagashima, Y. Niwa, *J. Inorg. Nucl. Chem.* **1978**, *40*, 789–791.
- [46] L.-F. Song, C.-H. Jiang, C.-L. Jiao, J. Zhang, L.-X. Sun, F. Xu, W.-S. You, Z.-G. Wang, J.-J. Zhao, *Cryst. Growth Des.* **2010**, *10*, 5020–5023.
- [47] O. Yaghi, H. Li, T. Groy, *J. Am. Chem. Soc.* **1996**, *118*, 9096–9101.
- [48] D. Sheberla, L. Sun, M. A. Blood-Forsythe, S. Er, C. R. Wade, C. K. Brozek, A. Aspuru-Guzik, M. Dincă, *J. Am. Chem. Soc.* **2014**, *136*, 8859–8862.
- [49] A. A. Talin, A. Centrone, A. C. Ford, M. E. Foster, V. Stavila, P. Haney, R. A. Kinney, V. Szalai, F. El Gabaly, H. P. Yoon, *Science* **2014**, *343*, 66–69.
- [50] H. Yin, C. Zhang, F. Liu, Y. Hou, *Adv. Funct. Mater.* **2014**, *24*, 2930–2937.

Received: August 4, 2016

Published online: October 24, 2016